# Development of Disaster Mitigation Approach and Coastal Area Carrying Capacity Based on Coastal Vulnerability Index (CVI): A GIS Analysis in Betahwalang Waters, Demak

Galung Dhiva Maharani[1,3,4], Agus Indarjo[1*], Muhammad Zainuri[2,3,4], Denny Nugroho Sugianto[2,3,4], Baskoro Rochaddi[2] , Dwi Haryo Ismunarti[2], Indra Budi Prasetyawan[2], Nazariano Rahman Wahyudi[2], Chrisna Adhi Suryono[1], Bambang Yulianto[1], Ria Azizah Tri Nuraini[1], Fadhil Muhammad[1]

[1]Department of Marine Science, Faculty of Fisheries and Marine Science, Universitas Diponegoro
[2]Department of Oceanography, Faculty of Fisheries and Marine Science, Universitas Diponegoro
Jl. Prof. Jacub Rais, Tembalang, Semarang, Central Java, 50275 Indonesia
[3]Center for Coastal Rehabilitation and Disaster Mitigation Studies, Universitas Diponegoro
[4]Integrated Laboratory for Research and Services, Universitas Diponegoro
Jl. Prof. Soedarto, SH, Tembalang, Semarang, Central Java, 50275 Indonesia
Email: agusindarjo@lecturer.undip.ac.id

*Abstract*

*This study aims to develop an integrated framework for disaster mitigation and coastal carrying capacity assessment by combining the Coastal Vulnerability Index (CVI) with trophic status analysis in Betahwalang Waters, Demak. Unlike previous studies that primarily evaluate physical vulnerability or ecological conditions separately, this study integrates both approaches to identify areas where high physical susceptibility coincides with ecological pressure, thereby providing a more comprehensive basis for sustainable coastal management. Seven physical parameters, including geomorphology, slope, elevation, land use, distance from the shoreline, distance from rivers, and tidal range, were analyzed using a weighted overlay approach in ArcGIS based on field observations, Sentinel-2 imagery, Digital Elevation Model (DEM), and tidal data. Ecological carrying capacity was assessed using trophic status derived from chlorophyll-a and nitrate concentrations following the EPA trophic classification. The results indicate that 69.01% of the study area falls within the high (42.96%) and very high (26.05%) coastal vulnerability classes, primarily due to low elevation, gentle slopes, and extensive aquaculture replacing natural mangrove protection. Chlorophyll-a concentrations ranged from 2.19 to 36.19 μg.L$^{-1}$, while nitrate concentrations ranged from 43.62 to 126.52 μg.L$^{-1}$, indicating mesotrophic to eutrophic conditions with moderate to high nutrient enrichment. The integrated assessment revealed that physically vulnerable areas generally coincide with nutrient-enriched coastal waters, indicating increasing environmental pressure and reduced ecological carrying capacity. These findings demonstrate that integrating CVI with trophic status provides additional spatial insight beyond conventional vulnerability assessments by simultaneously identifying priority areas for ecosystem restoration, disaster risk reduction, and sustainable aquaculture management. The integration of CVI and trophic status provides additional spatial insight by identifying areas where high physical vulnerability coincides with ecological pressure, thereby supporting ecosystem-based disaster mitigation and sustainable coastal management. The proposed framework supports evidence-based coastal planning through ecosystem-based disaster mitigation strategies, including mangrove restoration, spatial zoning, and adaptive coastal management under climate change.*

***Keywords:*** *Coastal vulnerability, Trophic status, Disaster mitigation, Betahwalang*

## Introduction

The northern coast of Java, Indonesia, is among the most hazard-prone regions, frequently exposed to coastal processes such as tidal flooding (rob), shoreline erosion, and sea-level rise. Tidal flooding (rob) that occur disrupts livelihoods and damages infrastructure, particularly in low-lying coastal villages such as Sayung, Timbulsloko, and Bedono in Demak Regency, where recurrent inundation has impacted aquaculture activities, transportation access, and housing conditions (Marfai and King, 2008; Zainuri *et al.*, 2024). The flat geomorphology and low elevation of this coastal plain increase the vulnerability of aquaculture ponds, coastal infrastructure, and scattered settlements to hydrometeorological hazards, particularly tidal inundation (rob) and shoreline change driven by coastal processes rather than pluvial rainfall (Simbolon, 2016; Maulina and Sulastri, 2020). In

*) Corresponding author

https://ejournal.undip.ac.id/index.php/ijms
DOI: 10.14710/ik.ijms.31.3.333-352
Received : 04-06-2026
Accepted : 07-08-2026

Demak Regency, these hazards are intensified by land subsidence driven due to the excessive groundwater extraction and anthropogenic land-use changes.

Demak's coastal area supports diverse land uses such as mangrove forests, aquaculture ponds, rice fields, and settlements yet this multifunctional landscape is highly vulnerable to environmental degradation, particularly mangrove deforestation, aquaculture expansion, and land subsidence driven by anthropogenic activities (Wirasatriya *et al*., 2019). Changes in monsoonal wind regimes and hydro-oceanographic dynamics affect shoreline stability and tidal inundation (Bosboom and Stive, 2015). Continuous rob events, combined with mangrove loss and sedimentation, have led to ecosystem decline and reduced coastal resilience. Approximately 252 ha of mangrove forests in Demak are in a critical condition, weakening natural coastal protection and nutrient cycling (Azizah *et al.,* 2018).

The proposed Giant Sea Wall along the North Coast of Java aims to mitigate tidal flooding but faces criticism for addressing symptoms rather than root causes such as subsidence and ecosystem loss (Anthony *et al.,* 2015). Structural interventions without ecological restoration may disrupt coastal hydrology, reduce mangrove habitats, and negatively affect fisheries and local livelihoods. Therefore, integrated and adaptive approaches that combine ecological restoration, hydrological control, and spatial management are required for long-term resilience (Sarwar and Woodroffe, 2013).

To support targeted disaster mitigation, assessing coastal vulnerability and aquatic productivity provides essential scientific input for identifying priority areas where high physical exposure coincides with ecological stress, thereby informing the need and type of intervention. The Coastal Vulnerability Index (CVI) offers a quantitative framework for evaluating physical susceptibility using parameters such as geomorphology, slope, elevation, tidal range, and distance from the shoreline and rivers (Darmawan *et al.,* 2021). Meanwhile, trophic classification based on chlorophyll-a and nitrate concentrations indicates water productivity and nutrient enrichment. While the Coastal Vulnerability Index (CVI) identifies areas that are physically susceptible to coastal hazards, it does not provide information on the ecological condition of coastal waters. Conversely, trophic status reflects nutrient dynamics and aquatic productivity but does not indicate the degree of physical exposure to coastal hazards. Therefore, integrating these two indicators enables a more comprehensive assessment by simultaneously evaluating physical susceptibility and ecological resilience, allowing management priorities to be identified based on both disaster risk and ecosystem condition (Wieder *et al.,* 2013; Woodruff *et al.,* 2013; Valdez-Rojas *et al.,* 2022). Integrating these two methods provides a complementary perspective by distinguishing areas of high physical exposure (CVI) from zones of ecological stress (trophic status), thereby supporting more targeted disaster mitigation strategies and ecosystem-based management in Betahwalang Waters, Demak (Noyiantoro *et al.,* 2022). Unlike previous studies that primarily assess physical coastal vulnerability or ecological conditions independently, this study integrates GIS-based Coastal Vulnerability Index (CVI) mapping with trophic status assessment within a unified spatial assessment framework. This approach enables the identification of areas where high physical vulnerability coincides with ecological pressure, thereby providing additional information for prioritizing ecosystem restoration, disaster mitigation, and sustainable coastal management.

Recent advances in GIS-based coastal vulnerability assessment have shifted from conventional physical parameter mapping toward more integrated frameworks that incorporate ecological, socio-environmental, and environmental quality indicators to better represent the complexity of coastal systems (Mishra *et al.,* 2023). These developments demonstrate that combining physical vulnerability with ecological conditions can improve the identification of priority areas for ecosystem restoration, disaster risk reduction, and sustainable coastal management (McLachlan and Dorvlo, 2005; Isdianto *et al.,* 2021; Ma'rufatin *et al.,* 2024). However, most previous studies have focused on either physical vulnerability or ecological conditions independently, with limited efforts to integrate both perspectives within a unified spatial assessment framework.

This study aims to (1) analyze GIS-based physical and environmental parameters as inputs for disaster mitigation through the CVI and trophic classification; (2) analyze the spatial distribution of vulnerability levels alongside trophic status derived from chlorophyll-a and nitrate concentrations; and (3) examine the relative influence of selected parameters within the CVI framework to support interpretation of spatial vulnerability patterns, rather than to develop a new weighting scheme.

The research contributes to sustainable coastal management and national policy implementation, particularly Presidential Regulation No. 83/2018 on Marine Waste Management and Ministerial Decree No. 38/2024 on Betahwalang Marine Conservation Area. The combined CVI–trophic approach provides a scientific basis for identifying high-risk zones, assessing ecosystem health, and guiding adaptive strategies for disaster risk reduction and sustainable coastal management. Furthermore, the findings align with the Sustainable Development Goals (SDGs)—notably SDG 13 (Climate Action), SDG 14 (Life Below Water), and SDG 15 (Life on Land)—by promoting integrated coastal zone management that balances environmental sustainability, community welfare, and disaster mitigation.

## Materials and Methods

### *Data Collection and Survey Design*

This research employed a combination of field-based measurements and spatial data analysis to evaluate the coastal vulnerability of Betahwalang Waters, Demak Regency. Primary data were collected through systematic field surveys at selected coastal segments to obtain direct observations of geomorphological features and to verify the accuracy of spatial interpretations (Hamuna *et al.,* 2018; Handiani *et al.,* 2019). Field assessments included the identification of coastal landforms, vegetation types, and protective structures such as mangrove belts and embankments.

Topographic profiles were measured using Real-Time Kinematic (RTK) GPS along selected coastal transects to obtain high-resolution elevation data. The RTK survey was conducted by traversing along the coastline to capture detailed slope and elevation variations. These field measurements were used to validate and complement slope values derived from a Digital Elevation Model (DEM), which was processed in a GIS environment to generate a continuous slope map across the study area. In the spatial analysis stage, RTK-derived data were overlaid with DEM data in ArcGIS to produce a comprehensive slope representation for the entire Betahwalang area and its surroundings. The resulting slope data were then classified and incorporated as one of the parameters in the Coastal Vulnerability Index (CVI) analysis (Ringor and Siringan, 2016).

Secondary datasets included bathymetric data obtained in raster format from tanahair.indonesia.go.id, which were processed within a GIS environment to derive nearshore depth characteristics (Shi *et al.,* 1999; Pardo-Pascual *et al.,* 2012; Thanjaya and Saputra, 2021). The data were preprocessed through interpolation and clipping to match the study area extent and were subsequently used to support the analysis of coastal morphology and shoreline conditions within the Coastal Vulnerability Index (CVI) framework. Additional datasets comprised Sentinel-2 multispectral imagery acquired from USGS EarthExplorer, Digital Elevation Models (DEM) provided by the Geospatial Information Agency (BIG), and tidal observations obtained from the Meteorological, Climatological, and Geophysical Agency (BMKG). All spatial datasets were extracted and standardized according to the geographic extent of the Betahwalang coastal zone (Hammar *et al.,* 2003; Capobianco *et al.,* 2016).

### Data Preparation and Image Enhancement

To ensure data uniformity and reliability, all satellite-derived datasets underwent pre-processing prior to spatial analysis (Ehrhardt, 1999; Dong *et al.,* 2021; Bailey, 2025). Sentinel-2 imagery was corrected atmospherically using the Semi-Automatic Classification Plugin (SCP) within ArcGIS 10.8 to minimize haze and radiometric distortion. Only imagery with less than 10% cloud cover was selected. The Normalized Difference Water Index (NDWI) algorithm was applied to delineate surface water features and extract the boundary between land and water bodies, thereby approximating the land–water interface. As NDWI does not differentiate between water body types, the resulting classification was further refined through visual interpretation, GIS-based spatial analysis, and elevation data from the DEM to better represent the shoreline position (Ridarto *et al.,* 2026).

DEM data were standardized to a 10-meter spatial resolution to maintain consistency across all layers. Meanwhile, tidal data were averaged for the 2024–2025 period to represent mean tidal dynamics and minimize seasonal bias. These preprocessing steps ensured the spatial integrity and analytical precision of subsequent geospatial assessments (Capobianco *et al.,* 2016).

### *Geospatial Processing and Analytical Framework*

All spatial analyses were conducted within a GIS environment using a structured workflow to ensure consistency across datasets. The analysis began with the preparation of spatial input layers, including geomorphology, coastal slope, elevation, land use, distance from shoreline, distance from river, and tidal range. Distance-based parameters (distance from shoreline and river) were generated using buffer analysis, in which multiple distance zones were created to represent varying levels of exposure. All input layers were converted into raster format with a consistent spatial resolution and extent. Each parameter was then reclassified into standardized vulnerability classes based on predefined thresholds, assigning scores ranging from low to very high vulnerability. The weighting scheme for each parameter followed established CVI approaches, where relative importance was assigned based on literature and coastal process relevance (Ariffin *et al,* 2023).

A weighted overlay analysis was subsequently applied by combining all reclassified raster layers according to their respective weights to produce a composite Coastal Vulnerability Index (CVI) map. This process involved multiplying each raster layer by its assigned weight and summing the results to generate a spatially explicit vulnerability index (Furlan *et al.,* 2021). The final CVI values were then classified into vulnerability categories (low, moderate, high, and very high) for interpretation (Table 1). In parallel, trophic status was analyzed using chlorophyll-a and nitrate data, which were spatially interpolated and classified into trophic categories. The integration of CVI and trophic results was conducted through spatial comparison to identify areas where high physical vulnerability coincides with elevated ecological pressure.

*Parameter Weighting and Analytical Justification*

The selection of parameters: geomorphology, coastal slope, elevation, land use, distance from shoreline, distance from river, and tidal range was based on their established relevance in influencing coastal vulnerability in low-lying deltaic environments. The weighting scheme was adapted from established Coastal Vulnerability Index (CVI) frameworks (e.g., Gornitz, 1991), where parameter importance reflects their influence on coastal processes. Rather than applying statistical methods such as AHP, weights were assigned based on process-based understanding to ensure physical relevance.

The weighting scheme adopted in this study was based on previous Coastal Vulnerability Index (CVI) frameworks reported in the literature (Gornitz, 1991; Hamuna *et al.,* 2018; Pantusa *et al.,* 2018). Higher weights were assigned to geomorphology and coastal slope because these parameters exert a stronger influence on coastal susceptibility by controlling shoreline stability and inundation potential. Intermediate weights were assigned to elevation, distance from the shoreline, distance from rivers, and tidal range, while land use received a lower weight as it primarily represents anthropogenic modification rather than intrinsic physical susceptibility.

Although the study area extends more than 1000 m inland, it remains part of a coastal system due to tidal flooding (rob), land subsidence, and strong hydrological connectivity between the sea, rivers, and aquaculture ponds. In this context, distance-based parameters represent gradients of exposure rather than strict coastal proximity (Pantusa *et al.,* 2018; Ramadhani, 2025). Geomorphology and slope were assigned higher weights due to their control on coastal resistance and the inland propagation of inundation, particularly under uniformly low slopes (0–2%). Elevation is critical as most of the area lies below 1.8 m, increasing susceptibility to flooding. Distance from shoreline represents exposure to marine forcing, while distance from river reflects fluvial–coastal interactions affecting water distribution in pond-dominated areas (Castro *et al.,* 2020; Karasius *et al.,* 2024). Tidal range was included as a modifying factor influencing inundation extent, as tidal signals propagate inland through channels and low-lying terrain.

Overall, the weighting reflects process-based controls in a low-gradient, subsiding, and hydrologically connected system, and is intended to support spatial interpretation of vulnerability rather than absolute risk quantification.

*Computation of the Coastal Vulnerability Index (CVI)*

The Coastal Vulnerability Index was computed using a Weighted Linear Combination (WLC) model that integrates all normalized parameters according to the following equation (Darmawan *et al.,* 2017; Pantusa *et al.,* 2018; Ramadhani, 2025):

$$CVI = \Sigma Wi \times Si = (20 \times G) + (20 \times S) + (15 \times E) + (15 \times DfS) + (15 \times DfR) + (10 \times TR) + (5 \times LU)$$

Note: CVI = Coastal Vulnerability Index; Wi = weight assigned to each parameter i (expressed as a percentage); Si = score representing the vulnerability class of each parameter; G = geomorphology; S = slope; E = elevation; DfS = distance from shoreline; DfR = distance from river; TR = tidal range; LU = land use.

Where Wi represents the assigned weight (%) of parameter i and S_i its corresponding vulnerability score. Tidal range was incorporated as a non-spatial parameter using observed monthly tidal data, represented as a uniform value across the study area. Due to the absence of spatially distributed tidal data, this parameter was converted into a constant raster layer and classified based on CVI thresholds. The resulting layer was included in the weighted overlay analysis to represent the overall influence of tidal forcing on coastal vulnerability. The computed CVI values were classified into five categories—very low, low, moderate, high, and very high—using the Natural Breaks (Jenks) method in ArcGIS. Each spatial cell was subsequently color-coded to produce the final Coastal Vulnerability Map for Betahwalang Waters (Figure 1).

**Table 1.** Score and Weight for Each Coastal Vulnerability Criterion

| Variables | Score | | | | | Weight |
|---|---|---|---|---|---|---|
| | Very Low | Low | Medium | High | Very High | |
| | 1 | 2 | 3 | 4 | 5 | |
| Geomorphology (G) | Stony and hilly beach | Medium clifffed beach | Low cliffed-beach, glacial flow | Stony beach, estuary, lagoon | Barrier beach, sandy beach, delta | 20% |
| Slope (S) | >12% | 8 - 12% | 4 - 8% | 2 - 4% | <2% | 20% |
| Elevation (E) | >3.4 m | 3.0 - 3.4 m | 2.5 - 3.0 m | 1.8 - 2.5 m | <1.8 m | 15% |
| Distance from shoreline (DfS) | >1000 m | 750 - 1000 m | 500 - 750 m | 250 - 500 m | 0 - 250 m | 15% |
| Distance from River (DfR) | >400 m | 300 - 400 m | 200 - 300 m | 100 - 200 m | 0 - 100 m | 15% |
| Tidal Range (TR) | <0.2 m | 0.2 - 0.4 m | 0.4 - 0.6 m | 0.6 - 0.8 m | >0.8 m | 10% |
| Land use (LU) | Mangrove forest | Plantation, farm | Open Field, scrub | Built land, house, buildings | River, pond | 5% |

Source: Darmawan *et al.* (2017); Pantusa *et al.* (2018); Ramadhani (2025)

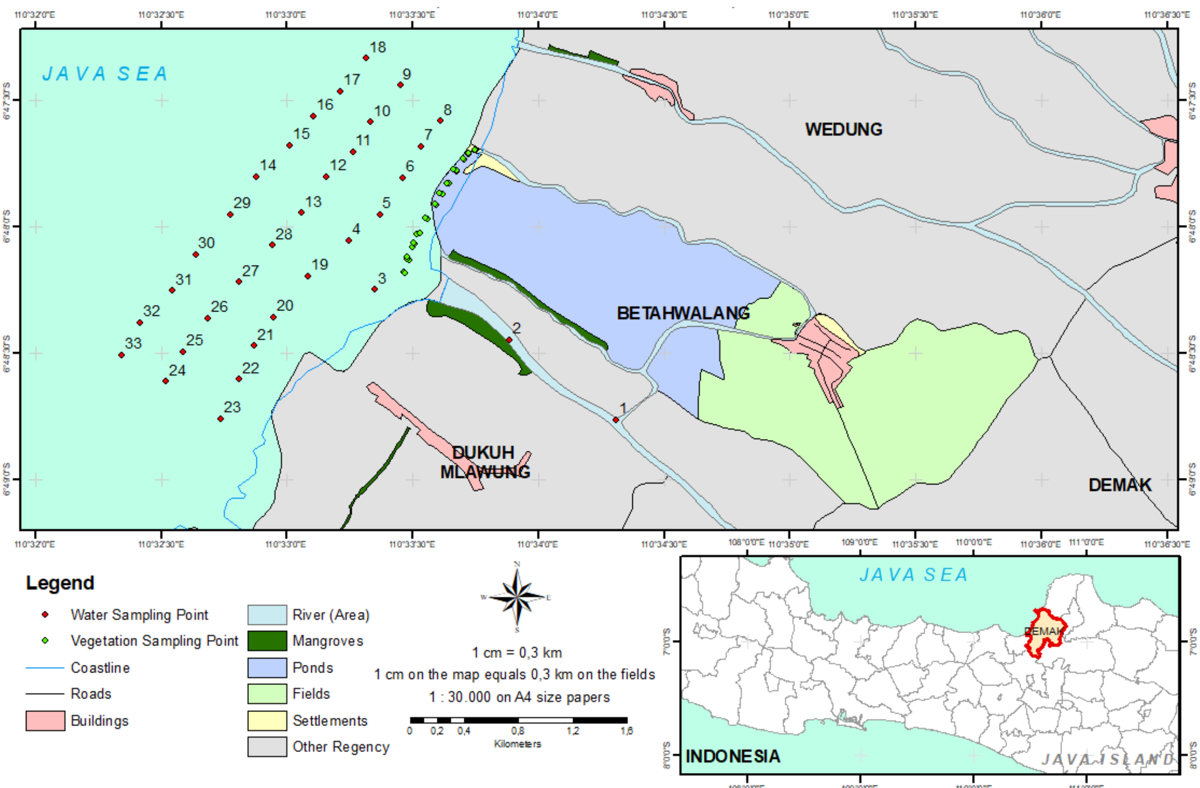


**Figure 1.** Research Location: Betahwalang Waters, Demak Regency

### *Model Validation and Reliability Assessment*

The reliability of the CVI model was evaluated through field verification and comparison with historical records of tidal inundation and shoreline retreat. Areas classified as high and very high vulnerability generally corresponded with observed erosion zones and frequently flooded sites, indicating consistency between model outputs and known field conditions. This correspondence is expected, as the CVI framework emphasizes key physical controls such as elevation, slope, and proximity to coastal and fluvial systems. However, it is important to note that these parameters represent inherent susceptibility rather than dynamic exposure to hydrodynamic forcing. As such, the CVI results are intended to identify relative vulnerability patterns and spatial trends, rather than to directly model the processes driving inundation and erosion. Quantitative validation was further performed by comparing CVI outputs with geomorphological and hydrodynamic observations (Darmawan *et al.,* 2017; Handiani *et al.,* 2019; Valdez *et al.,* 2019; Ariffin *et al.,* 2023). The strong spatial agreement between modeled and observed conditions demonstrates the robustness and predictive validity of the CVI approach for assessing coastal hazard exposure in Betahwalang Waters.

The trophic status of the Betahwalang coastal waters was determined using the Trophic State Index (TSI) approach adopted from the U.S. Environmental Protection Agency (EPA). This method classifies aquatic systems based on nutrient enrichment and primary productivity, particularly chlorophyll-a and nitrate concentrations (Hindaryani *et al.,* 2020; Widiaratih *et al.,* 2022). The classification provides an ecological assessment of water fertility and eutrophication potential. In this study, trophic categorization was simplified to reflect chlorophyll-a and nitrate ($NO_3^-$) concentrations, following EPA-based classification thresholds. Water quality data were collected from 33 sampling stations distributed across the study area, with observations conducted during two different seasonal periods, namely 27th April 2025 and 19th October 2025, representing contrasting coastal conditions. This two-period sampling approach, with an interval of approximately seven months, was applied to account for temporal variability in coastal water conditions (Basuki *et al.,* 2024). The results indicate that trophic index values and classification levels between the two sampling periods show no significant differences and tend to be consistent, suggesting relatively stable nutrient conditions within the study area. While acknowledging that marine phytoplankton dynamics can exhibit high temporal variability, the use of multi-period observations in this study provides a more representative assessment compared to single-time sampling. The resulting trophic classification is therefore interpreted as an indicative assessment of general water fertility conditions rather than a fully resolved seasonal characterization.

### *Chlorophyll-a Determination*

The concentration of chlorophyll-a was analyzed using the spectrophotometric method following the protocol of the APHA (2012) standard. From each station, a fixed volume of 1 L of seawater was filtered through a 0.45 μm cellulose membrane filter (47 mm diameter) using a vacuum filtration system. All samples were successfully filtered without filter clogging, ensuring a consistent filtration volume for chlorophyll-a determination. Three drops of 0.12 M $MgCO_3$ solution were added during filtration to maintain slightly alkaline conditions, thereby minimizing the conversion of chlorophyll-a to pheophytin and preserving pigment stability during extraction. The following steps were performed sequentially: The filter containing the retained pigments was transferred into a centrifuge tube and extracted with 10 mL of 90% acetone. The samples were then stored at 4°C for 16–24 hours to ensure complete pigment extraction. After the extraction period, the samples were centrifuged at 4000 rpm for 10 minutes to separate the supernatant, and the absorbance of the resulting supernatant was measured using a UV–Vis spectrophotometer at wavelengths of 664, 647, and 630 nm.

The chlorophyll-a concentration (Chl-a) was calculated using the formula:

$$Chl - a\ (mg.L^{-1}) = \frac{\mathrm{Ca\ x\ Va}}{\mathrm{V\ x\ d}}$$

Note: $Ca = 11.85E664 - 1.54E647 - 0.08E630$;
Va = volume of acetone (mL); V = volume of filtered water sample (L); d = path length of the cuvette (cm); E = absorbance at respective wavelengths

This procedure ensured accurate quantification of chlorophyll-a as a proxy for phytoplankton biomass and primary productivity in the study area. To facilitate reproducibility, all spatial datasets were projected to WGS 84 / UTM Zone 49S prior to analysis. Raster layers were standardized using a common spatial resolution before applying the weighted overlay analysis in ArcGIS 10.8. The analytical workflow, including parameter scoring, weighting, overlay analysis, and trophic classification, was consistently applied to all datasets following the procedures described above.

### *Nitrate Determination*

The analytical procedure was performed according to the original method described by Parsons *et al.* (1984). The principle of this method involves the reduction of nitrate ($NO_3^-$) to nitrite ($NO_2^-$) by a cadmium column coated with copper, followed by colorimetric detection. The analytical steps were as follows: The water samples were divided into two subsamples for total nitrate and nitrite determination. The nitrate subsample was treated with concentrated $NH_4Cl$ reagent and passed through a cadmium reduction column to convert nitrate ($NO_3^-$) into nitrite ($NO_2^-$). Subsequently, both subsamples were reacted with sulfanilamide under acidic conditions to form a diazonium compound, which was then coupled with N- (1-naphthyl)-ethylenediamine dihydrochloride (NED) to produce a pink azo dye. The absorbance was measured at 543 nm using a Hitachi U-2900 UV–Vis spectrophotometer

**Table 2.** Trophic State, Constituent Concentrations, and Use of Water Bodies (Environmental Protection Agency, United States)

| Trophic Category | Chlorophyll-a (μg.L$^{-1}$) | Nitrate (μg.L$^{-1}$) | Description |
|---|---|---|---|
| Oligotrophic | < 3 | < 400 | Low productivity; clear water, minimal algal biomass |
| Mesotrophic | 3–7 | 400–600 | Moderate productivity; balanced nutrient levels |
| Eutrophic | 7–40 | 600–1500 | High productivity; potential algal blooms |
| Hypertrophic | > 40 | > 1500 | Very high productivity; frequent eutrophication events |

This classification facilitates the assessment of ecological health, identifies nutrient-enriched zones, and supports management planning for coastal ecosystem sustainability.

(Hitachi High-Tech Corporation, Tokyo, Japan). The analysis followed the standardized laboratory procedure described by Parsons *et al.* (1984). Atomic nitrogen concentration (μg atom N/L) was calculated using the equation:

$$N = (Ared - Anonred)x\,F$$

Where:

$$F = \frac{20}{\mathrm{Es}}$$

represents the absorbance ratio between the standard and blank solutions. The nitrate concentration was subsequently converted to mg.L$^{-1}$ using the equation:

Nitrate (mg.L$^{-1}$) = (N × 14)/1000.

sensitivity for low nitrate concentrations and was suitable for detecting nutrient gradients associated with anthropogenic input in coastal waters.

### *Integration of Trophic Metrics*

Chlorophyll-a and nitrate data were used as key indicators of primary productivity and nutrient conditions; however, it is acknowledged that these parameters alone are insufficient to fully characterize the trophic status of aquatic ecosystems, and therefore provide only a partial assessment of nutrient enrichment. Spatial variations were analyzed to distinguish areas of nutrient enrichment and potential eutrophication (Carlson, 1977). Stations with higher chlorophyll-a and nitrate concentrations were classified as eutrophic to hypertrophic, while those with lower values were designated as oligotrophic or mesotrophic (Table 2) (Anderson *et al.,* 2002). This integrated approach provided an indicative assessment of spatial patterns in biological productivity, which may serve as a preliminary reference for coastal management. However, it is acknowledged that comprehensive evaluation of ecological conditions would require long-term monitoring and more frequent sampling to capture temporal variability.

In this study, coastal carrying capacity was evaluated qualitatively using trophic status as an ecological indicator representing the capacity of coastal waters to sustain primary productivity under existing nutrient conditions.

### *AI Usage Disclosure Statement*

Artificial intelligence (AI) tools were used in a limited and supportive manner during the preparation of this manuscript. Specifically, AI-based language assistance (i.e., ChatGPT by OpenAI) was utilized to improve grammatical accuracy, clarity of expression, and overall readability of the text. The AI tools did not generate original scientific content, research data, analyses, interpretations, or conclusions. All research design, data collection, data analysis, result interpretation, and scientific arguments were conducted independently by the authors. The authors take full responsibility for the content of this manuscript and confirm that the use of AI complies with the journal's ethical guidelines, transparency requirements, and publication standards.

## Result and Discussion

The Coastal Vulnerability Index (CVI) map produced in this study illustrates the spatial distribution of coastal susceptibility to tidal inundation, shoreline change, and associated hydrodynamic processes in Betahwalang, as determined by the integration of key physical and environmental parameters (Appeaning 2011). This approach combines several physical and environmental variables into a composite index. The resulting CVI values were classified into five categories such as Very Low, Low, Moderate, High, and Very High that representing relative susceptibility to tidal inundation and shoreline change (Figure 1-2). Classification was conducted using the Natural Breaks (Jenks) method, which minimizes within-class variance and maximizes between-class differences, making it suitable for spatial datasets with non-uniform distributions. The numerical ranges associated with each class are provided to ensure transparency and interpretability of the classification—to facilitate spatial interpretation and coastal management planning (Alongi, 2008). The subsequent figures illustrate the processed results of each parameter: geomorphology, land use, elevation, slope, distance from coastline, distance from river, and tidal range. These layers were analyzed using a weighted overlay method, producing the final coastal vulnerability map for the Betahwalang area (Darmawan *et al.,* 2017).

The CVI results reveal that spatial variations in coastal vulnerability in Betahwalang are predominantly controlled by elevation, slope, and proximity to the shoreline and river systems, which influence the extent of tidal inundation and shoreline change across the study area (Ramadhani, 2025).

Assessing the trophic status of coastal waters provides essential insight into the nutrient dynamics and productivity levels that influence ecosystem health and resilience. In this study, trophic classification was determined based on the concentrations of chlorophyll-a and nitrate, which serve as primary indicators of phytoplankton biomass and nutrient enrichment, respectively. Elevated concentrations of these parameters generally reflect higher nutrient inputs, often resulting from terrestrial runoff or anthropogenic activities, and can indicate eutrophication processes in coastal systems (Noyiantoro *et al.,* 2022; Basuki *et al.,* 2024). The analysis aimed to categorize the Betahwalang coastal waters into trophic levels—oligotrophic, mesotrophic, eutrophic, or hypertrophic—to evaluate the degree of water fertility and identify potential ecological pressures. The following subsections present and interpret the spatial distribution of key physical and environmental parameters contributing to the CVI, emphasizing their role in shaping coastal vulnerability patterns across the study area (Hindaryani *et al.,* 2020).

### *Geomorphological Characteristics*

The coastal morphology of Betahwalang is largely defined by sandy beaches interspersed with several river estuaries, which are primarily distributed along the coastal margin of the study area. These geomorphological features correspond spatially with zones identified as having higher CVI values. Sandy shorelines in Betahwalang exhibit characteristics associated with dynamic coastal environments, where sediment redistribution and shoreline adjustment are evident from the spatial patterns observed in the CVI map. This condition is further reflected in areas where geomorphological units coincide with higher vulnerability classes, particularly in locations lacking natural protective features (Gornitz, 1991; Anggoro *et al.,* 2021).

Estuarine zones introduce additional spatial variability, as these areas function as transitional environments for tidal flow and sediment exchange. In the study area, estuarine sections are also associated with relatively higher CVI values, indicating their contribution to increased susceptibility to tidal influence and shoreline change. The combined occurrence of sandy coastal forms and estuarine systems results in a shoreline configuration that is more exposed compared to adjacent areas with relatively more stable conditions (Ringor and Siringan, 2016).

Furthermore, the limited presence of natural coastal buffers, such as mangrove vegetation, is reflected in the spatial distribution of higher vulnerability classes. Overall, the CVI results suggest that geomorphological characteristics play a significant role in controlling the spatial variability of coastal vulnerability in Betahwalang, particularly in relation to areas influenced by tidal processes and shoreline dynamics (Nurul *et al.,* 2025).

### *Land Use Characteristics*

Land use in Betahwalang is predominantly characterized by extensive fishponds occupying low-lying coastal areas, as shown in the land use map. These aquaculture zones are primarily distributed in areas that correspond with moderate to high CVI values, particularly in low-elevation zones exposed to tidal influence. The spatial pattern also indicates that areas where natural coastal ecosystems, such as mangroves, have been converted into fishponds tend to coincide with higher vulnerability classes (Irsadi, 2019; Zainuri *et al.,* 2024).

In addition, built-up zones, including settlements and infrastructure, are observed within areas classified as moderate to high vulnerability, reflecting their location within low-lying and tidally influenced environments. Conversely, the remaining mangrove stands are limited in spatial extent and are generally associated with relatively lower CVI values compared to surrounding aquaculture-dominated areas (Alongi, 2008).

Overall, land use variations show some association with the spatial distribution of CVI values; however, their influence is relatively minor compared to the dominant control of physical parameters such as elevation and slope.

### *Elevation Characteristics*

The topography of Betahwalang's coastal area is characterized by very low elevation, ranging between 0–1.8 meters above mean sea level, as shown in the elevation map. These low-lying conditions are spatially associated with areas classified as moderate to very high CVI values, particularly in zones closer to the coastline and river systems. Areas within the lowest elevation range tend to correspond with higher vulnerability classes, reflecting their greater susceptibility to tidal influence and water accumulation (Anthony *et al.,* 2015).

Inland areas with slightly higher elevation are limited in extent and generally correspond to relatively lower CVI values, although the difference is not pronounced due to the overall flat topography of the region. The spatial pattern indicates that even minor variations in elevation contribute to differences in vulnerability classification across the study area (Blum and Roberts, 2009).

Overall, elevation plays a significant role in controlling the spatial distribution of coastal vulnerability in Betahwalang, particularly in relation to tidal inundation processes and the persistence of water in low-gradient environments.

### *Slope Characteristics*

Betahwalang's terrain exhibits an extremely gentle slope, with coastal gradients ranging between 0–2% (approximately 0°–1.15°), as shown in the slope map. This very low-gradient condition is consistently distributed across most of the study area and is spatially associated with zones classified as moderate to very high CVI values (Anggoro *et al.,* 2021). Such conditions allow tidal water to spread across extensive aquaculture areas, including fish ponds, where water levels are influenced by tidal fluctuations and local drainage conditions. This results in prolonged water presence in low-lying zones, particularly in areas with limited drainage capacity.

Areas with uniformly gentle slopes tend to correspond with higher vulnerability classes, indicating that the lack of topographic gradient limits efficient water recession. The spatial pattern also shows that slope variability across the study area is minimal, yet this uniform flatness contributes significantly to the persistence of inundation. The combination of low elevation and gentle slopes demonstrates the strong interdependence among physical parameters influencing vulnerability to tidal inundation and shoreline change in the study area.

### *Distance From The Coast Characteristics*

Betahwalang lies within approximately 250 meters of the coastline in several sections of the study area, as illustrated in the locality and spatial distribution maps, highlighting its close proximity to coastal processes. These nearshore zones are spatially associated with areas classified as high to very high CVI values. Areas located within 250–500 meters from the coastline also show moderate to high vulnerability classes, indicating that coastal influence extends inland within the study area (Marfai and King, 2008).

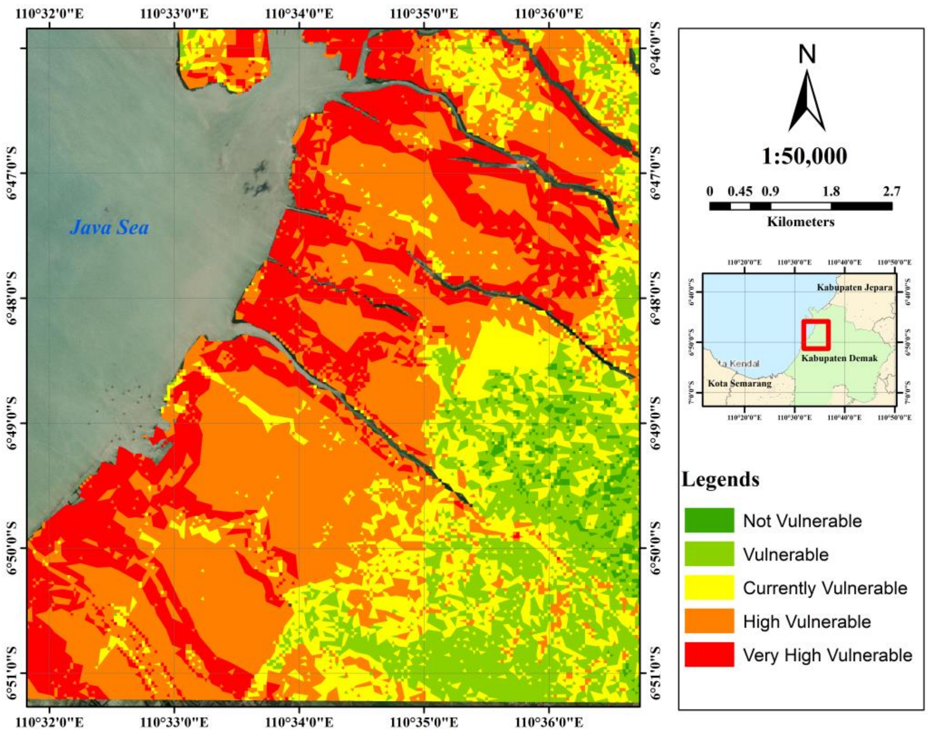


**Figure 3.** Coastal Vulnerability Map of the Research Area

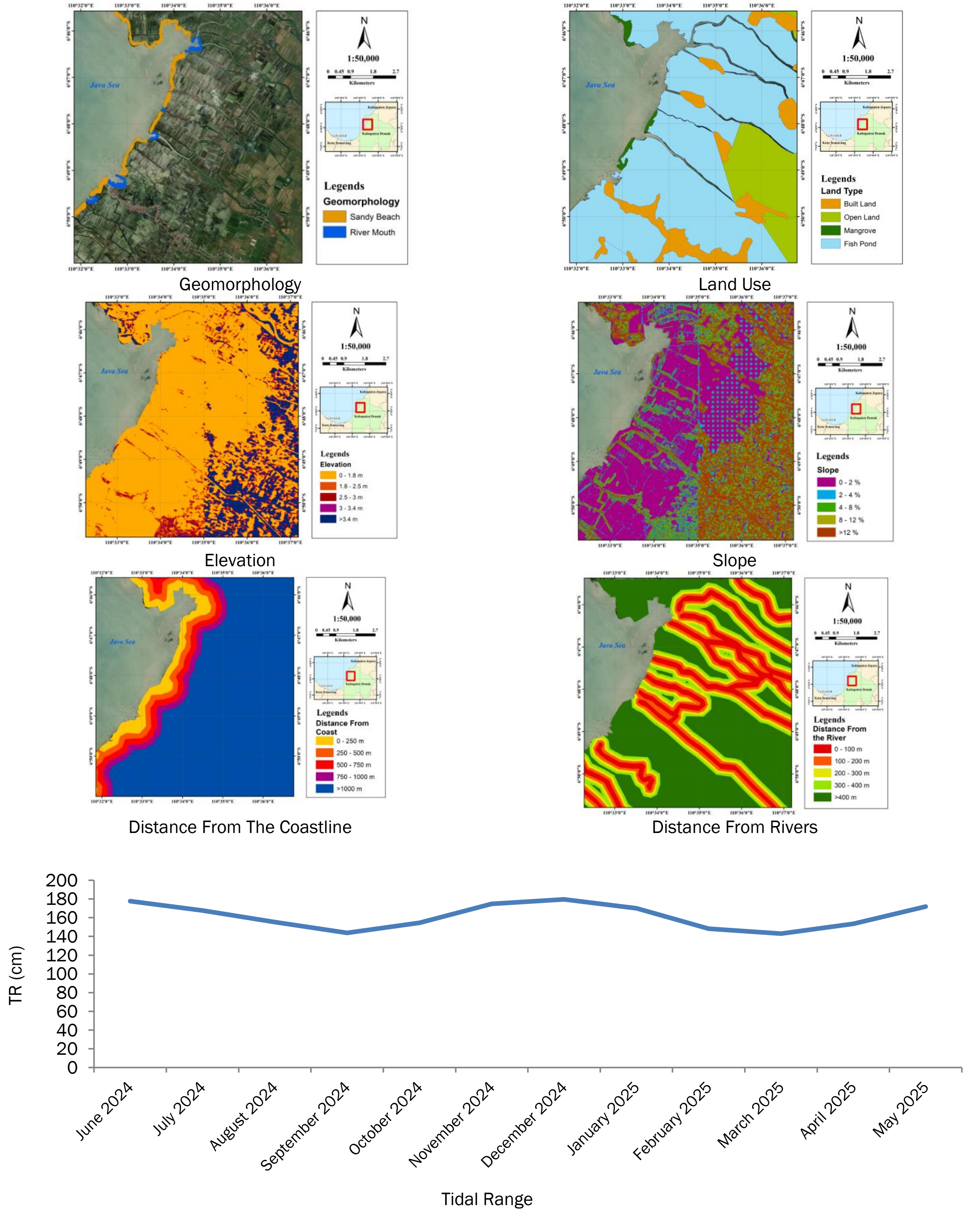


**Figure 2.** Spatial Distribution of Vulnerability Scores For Individual Coastal Vulnerability Index (CVI)

The spatial pattern demonstrates that proximity to the coastline is associated with increasing vulnerability levels, with areas closer to the shoreline generally corresponding to higher CVI values. This reflects the role of coastal proximity in influencing exposure to tidal processes and shoreline dynamics within the study area (de Sousa Júnior *et al.*, 2025; Zainuri *et al.*, 2024). Overall, distance from the coast contributes to the spatial variability of CVI values, particularly in delineating gradients of vulnerability between nearshore and more inland areas.

### *Distance From River Characteristics*

Betahwalang's landscape includes a dense river network, with many sites located within 100 meters of major river channels, as shown in the spatial distribution maps. Areas in close proximity to these river systems are generally associated with moderate to high CVI values, indicating their contribution to spatial variations in vulnerability. The spatial pattern suggests that river channels function as pathways for tidal water movement, allowing water to extend further inland, particularly in low-lying and aquaculture-dominated areas (Anthony *et al.,* 2015). Furthermore, saline water intrusion through river systems can influence water quality in aquaculture areas, particularly in fish ponds connected to tidal channels. Areas adjacent to rivers tend to correspond with higher vulnerability classes compared to more distant inland zones, reflecting the combined influence of fluvial and tidal processes. Overall, distance from river contributes to the spatial differentiation of CVI values, particularly in areas where hydrological connectivity facilitates the inland propagation of tidal influence.

### *Tidal Characteristics*

The tidal regime in Betahwalang displays a substantial range, with tidal amplitudes varying between 142.99 cm and 179.59 cm, as shown in the tidal observation data. The Highest High Water Level (HHWL) exceeding 90 cm indicates the potential for seawater to advance inland during high tides, particularly over low-lying terrain within the study area. This condition is reflected in areas classified with moderate to high CVI values, especially where low elevation and gentle slopes coincide (Zainuri *et al.,* 2024).

The interaction between relatively large tidal fluctuations and low-lying topography contributes to the spatial variability of vulnerability, particularly in zones influenced by tidal processes. However, as tidal range was applied as a uniform parameter in the analysis, its role is represented as a general influencing factor rather than a spatially variable component. Overall, tidal characteristics contribute to the interpretation of coastal vulnerability patterns in Betahwalang, particularly in relation to tidal inundation processes within low-gradient environments (Souza, 2025).

### *Chlorophyll-a Concentration (Phytoplankton Biomass)*

Chlorophyll-a concentrations across sampling stations in Betahwalang ranged from 2.19 to 36.19 $\mu g.L^{-1}$, reflecting spatial variability in phytoplankton biomass. Based on Environmental Protection Agency (EPA) classification, waters with <3 $\mu g.L^{-1}$ chlorophyll-a were categorized as oligotrophic, 3–7 $\mu g.L^{-1}$ as mesotrophic, 7–40 $\mu g.L^{-1}$ as eutrophic, and >40 $\mu g.L^{-1}$ as hypertrophic.

The majority of sampling points fall within the mesotrophic to eutrophic range, indicating moderate to relatively high levels of primary productivity (Yentsch and Menzel, 1963; Lorezen, 1967; Maharani *et al.,* 2024;). Higher chlorophyll-a values were observed near estuarine and mangrove-influenced areas, while lower concentrations were recorded at stations located further from these zones. This distribution corresponds with areas influenced by terrestrial inputs and aquaculture activities within the study area.

Spatially, chlorophyll-a distribution shows a gradient, with lower concentrations observed in more offshore locations and higher concentrations in nearshore zones (Hu *et al.,* 2012; Harding *et al.,* 1999; Werdel and Bailey 2002). This pattern reflects the influence of land–sea interactions and hydrological connectivity on the spatial distribution of phytoplankton biomass.

### *Nitrate Concentration and Nutrient Dynamics*

Nitrate concentrations ranged between 43.62 and 126.52 $\mu g.L^{-1}$, with the highest values recorded at nearshore and riverine stations. This spatial pattern corresponds with areas influenced by river inputs and aquaculture activities within the study area (Grasshoff *et al.,* 1999; MacIsaac and Dugdale, 1969). Higher nitrate concentrations are primarily observed in zones with stronger hydrological connectivity to land-based sources, while relatively lower values occur at stations located further offshore.

Despite generally higher nitrate concentrations nearshore, the relationship between nitrate and chlorophyll-a is not consistently linear across all sampling stations. Some locations exhibit moderate nitrate levels but relatively high chlorophyll-a concentrations, indicating variability in the response of phytoplankton biomass to nutrient availability (Howarth *et al.,* 1988; Bouwman *et al.,* 2009). This pattern suggests that nitrate distribution alone does not fully explain spatial variations in phytoplankton biomass, and that local environmental conditions, including light availability limited by suspended sediments, water temperature, and hydrodynamic mixing (current velocity), may influence the observed variability in productivity across the study area. In turbid coastal environments like Demak, high nutrient loads from river discharge are often not fully utilized by phytoplankton due to light limitation caused by high suspended solids (Cloern, 2001). Furthermore, strong tidal flushing can reduce the residence time of phytoplankton cells, preventing significant biomass accumulation despite high nutrient availability (Monbet, 1992).

### *Coastal Vulnerability Index (CVI) Classification*

The Coastal Vulnerability Index (CVI) analysis in Betahwalang Waters, Demak, integrates seven spatial parameters such as geomorphology, slope, elevation, distance from shoreline, distance from river, tidal range, and land use to represent relative patterns of coastal susceptibility (Couvillion *et al.,* 2017). The resulting CVI values were classified into five categories using the Natural Breaks (Jenks) method, which groups values based on inherent data distribution rather than equal intervals. While this approach facilitates visualization of spatial variability, the classification should be interpreted as relative rather than absolute levels of vulnerability.

The spatial distribution indicates that higher CVI values are concentrated in low-lying coastal zones and areas in close proximity to the shoreline and river systems, highlighting the combined influence of topographic and hydrological factors. In terms of areal extent, the High vulnerability class covers approximately 2,615.27 ha (42.96%), while the Very High class accounts for 1,585.73 ha (26.05%). Moderate vulnerability occupies 1,807.74 ha (29.70%), whereas Low and Very Low classes represent smaller proportions of 57.71 ha (0.94%) and 32.28 ha (0.53%), respectively. In contrast, Low and Very Low classes occupy only a marginal extent.

Field observations demonstrated that areas classified as having high and very high vulnerability generally corresponded with locations affected by tidal flooding, shoreline erosion, and low-lying topography, providing qualitative support for the spatial consistency of the CVI results. Nevertheless, the present assessment should be interpreted with caution, as uncertainties remain due to the adopted parameter weighting scheme, the spatial resolution of the input datasets, and the exclusion of dynamic coastal processes such as land subsidence, wave climate, and seasonal hydrodynamic variability (Ahmad and Haie, 2018).

This distribution suggests that the dominance of elevated CVI values is closely associated with the prevalence of low elevation, gentle slopes, and strong hydrological connectivity across the study area. However, it is important to note that these patterns are largely driven by the selected parameters and their assigned weights, which emphasize physical characteristics over dynamic forcing processes. As such, the CVI results primarily reflect spatial susceptibility based on static environmental conditions rather than direct exposure to specific coastal hazards.

These findings indicate that much of Betahwalang's coastal zone is characterized by relatively high susceptibility based on the combined influence of low elevation, gentle slopes, and proximity to shoreline and river systems. It is important to note that this susceptibility is derived from static physical parameters and does not explicitly quantify vulnerability to specific coastal hazards, but rather represents relative spatial patterns of potential exposure(Si Ringor and Siringan, 2016). The primary factors influencing this high vulnerability are low elevation, gentle coastal slopes, and proximity to the shoreline and river mouths. The flat topography (0–2% slope) allows tidal water to spread horizontally across wide areas during high tides or storm surges, particularly in low-lying deltaic environments.

Field observations confirm that the most vulnerable zones correspond to regions actively affected by tidal flooding, coastal erosion, and land subsidence (Sugianto *et al.,* 2022). The high correlation between modeled vulnerability and observed physical degradation indicates that the CVI approach provides a reliable tool for spatial risk assessment in low-lying tropical coasts such as Betahwalang. The observed spatial patterns indicate that coastal vulnerability in Betahwalang is primarily governed by the interaction between geomorphological characteristics and land-use change. The conversion of mangrove areas into aquaculture ponds reduces the natural buffering capacity of the coastline, thereby increasing its susceptibility to tidal inundation and shoreline erosion. These findings emphasize that coastal vulnerability is influenced not only by inherent physical characteristics but also by anthropogenic modifications that alter ecosystem resilience.

Parameter classification thresholds were established based on commonly adopted criteria in previous CVI studies and adjusted to the environmental characteristics of the study area. The final CVI values were classified using the Natural Breaks (Jenks) method, which groups observations according to inherent data distribution and minimizes within-class variance while maximizing differences among classes.

### *Trophic Classification and Ecosystem Productivity*

Rather than estimating carrying capacity through quantitative loading models, this study interpreted trophic status as an ecological proxy of coastal carrying capacity, allowing the integration of ecosystem condition with physical vulnerability. The trophic classification and assessment of ecosystem productivity in Betahwalang Waters are based on chlorophyll-a and nitrate measurements obtained during two sampling periods representing different seasonal conditions (April and October 2025) (Figure 4). These observations provide an indication of spatial variability in nutrient conditions and phytoplankton biomass; however, they should be interpreted as representative snapshots rather than long-term trends. By integrating chlorophyll-a and nitrate parameters, the trophic status of Betahwalang Waters was generally classified as oligotrophic to mesotrophic in offshore areas and mesotrophic to eutrophic in nearshore zones, particularly around river mouths and aquaculture-dominated areas (Harding *et al.,* 1999). This distribution indicates moderate to relatively high levels of productivity, with localized zones exhibiting elevated nutrient conditions. Spatial variations in chlorophyll-a and nitrate concentrations highlight the influence of local environmental factors, especially in areas with stronger hydrological connectivity to river inputs and aquaculture activities.

This pattern suggests that nitrate distribution alone does not fully explain spatial variations in phytoplankton biomass, and that local environmental conditions may influence the observed variability in productivity across the study area. Several ecological and biogeochemical mechanisms potentially explain this non-linear relationship. First, intensive biogeochemical cycles, such as nitrification and denitrification processes in these dynamic coastal waters, can rapidly alter the forms and availability of nitrogen. Second, the rapid nutrient cycling and high uptake rates by phytoplankton might deplete ambient nitrate concentrations rapidly, masking the actual nutrient enrichment status during sampling times. Third, phytoplankton growth is co-regulated by other limiting and shifting environmental factors in Betahwalang waters, including fluctuations in salinity from freshwater runoff, pH variations, water temperature, and seasonal rainfall patterns, which directly affect photosynthetic efficiency regardless of nitrate levels (Howarth *et al.,* 1988).

Despite these patterns, the relationship between nutrient concentrations and phytoplankton biomass is not consistently linear across all sampling stations, reflecting the complexity of processes governing primary productivity. Some areas with moderate nutrient concentrations exhibit relatively high chlorophyll-a values, suggesting the influence of additional environmental controls. The consistency of trophic classification between the two sampling periods indicates relatively stable conditions during the study timeframe, although the limited temporal coverage constrains the ability to capture broader seasonal variability and dynamic ecological responses (Table 3). Areas classified as eutrophic are generally associated with conditions of reduced water exchange and increased nutrient input, where phytoplankton accumulation may occur. Although no direct evidence of hypoxic conditions was observed during the sampling periods, the presence of localized eutrophic zones indicates the potential for ecological changes under sustained nutrient enrichment. These findings highlight the importance of continued observation to better understand temporal variability and trophic dynamics within the study area. The spatial coincidence of elevated nutrient concentrations with aquaculture-dominated and river-influenced areas suggests that land-based activities play an important role in shaping ecological conditions within the coastal waters. Consequently, nutrient enrichment should be interpreted as a cumulative response to hydrological connectivity and human activities rather than as an isolated indicator of ecosystem productivity.

However, since the trophic status in this study was inferred primarily from chlorophyll-a and nitrate concentrations, this ecological interpretation should be considered a baseline assessment. While these parameters serve as robust proxies for phytoplankton biomass and primary nutrient loading, a comprehensive trophic classification ideally requires other key indicators such as total phosphorus, total nitrogen, and water transparency (Secchi depth). Therefore, the observed eutrophic or mesotrophic tendencies in certain stations reflect localized nutrient enrichment and phytoplankton responses, but further comprehensive monitoring incorporating a wider suite of biogeochemical parameters is needed to fully characterize the ecosystem health of Betahwalang waters.

### *Management Implications and Recommendations*

The integration of CVI and trophic status in this study provides a spatial assessment framework that combines physical vulnerability with ecological conditions. Rather than evaluating these components independently, the integrated interpretation enables the identification of coastal areas where high physical susceptibility overlaps with nutrient-enriched waters, thereby supporting the prioritization of ecosystem restoration, disaster mitigation, and sustainable coastal management. The integration of Coastal Vulnerability Index (CVI) and trophic status (TSI) in this study provides a preliminary framework for identifying areas with differing levels of physical vulnerability and ecological conditions in Betahwalang Waters. Rather than serving as definitive management prescriptions, the results offer a spatially informed basis for considering potential management priorities (Ehler and Douvere; 2009). Areas classified as high to very high CVI and low to moderate trophic status are generally characterized by low ecological capacity and higher physical susceptibility, indicating zones

**Table 3.** Trophic Scores of Chlorophyll-a and Nitrate

| Station | Lat_Y | Lon_X | Chlorophyll-a ($\mu g.L^{-1}$) | Nitrate ($\mu g.L^{-1}$) |
|---|---|---|---|---|
| 1 | -6.812755166 | 110.5718137 | - | 126.07798 |
| 2 | -6.807495096 | 110.5647825 | - | 74.73914 |
| 3 | -6.804147748 | 110.555825 | 36.1936 | 34.88772 |
| 4 | -6.800897545 | 110.5541092 | 7.6882 | 19.8548 |
| 5 | -6.799216838 | 110.5561484 | 10.7785 | 13.40199 |
| 6 | -6.796774209 | 110.5576723 | 3.8732 | 7.37464 |
| 7 | -6.794712542 | 110.5589048 | 6.067 | 93.24665 |
| 8 | -6.793009425 | 110.5602045 | 5.0791 | 49.56609 |
| 9 | -6.790656434 | 110.5575154 | 3.8573 | 31.76768 |
| 10 | -6.793076653 | 110.5555658 | 4.1131 | 28.29309 |
| 11 | -6.795071092 | 110.5543781 | 4.6379 | 42.12054 |
| 12 | -6.796699918 | 110.5526296 | 5.3333 | 44.88603 |
| 13 | -6.799082381 | 110.5509943 | 13.7456 | 33.89498 |
| 14 | -6.796706981 | 110.5479914 | 5.2841 | 37.36957 |
| 15 | -6.794600494 | 110.5501651 | 10.7244 | 37.79503 |
| 16 | -6.792718102 | 110.5517338 | 6.6889 | 20.98936 |
| 17 | -6.791059804 | 110.5535265 | 3.482 | 14.67837 |
| 18 | -6.788863679 | 110.5552745 | 5.594 | 18.08205 |
| 19 | -6.803272945 | 110.55142 | 11.952 | 0.85092 |
| 20 | -6.805996445 | 110.5491252 | 5.9078 | 3.68732 |
| 21 | -6.807879418 | 110.5478242 | 4.8741 | 3.61641 |
| 22 | -6.81008497 | 110.5468375 | 4.0938 | 6.31099 |
| 23 | -6.812707317 | 110.5456384 | 13.6926 | 7.94192 |
| 24 | -6.810222544 | 110.541997 | 2.9572 | 3.90005 |
| 25 | -6.808284072 | 110.5431384 | 10.1307 | 18.72024 |
| 26 | -6.806029306 | 110.5447644 | 6.0972 | 45.52422 |
| 27 | -6.803653906 | 110.5468261 | 7.6922 | 32.12223 |
| 28 | -6.801233687 | 110.549067 | 8.5225 | 18.50751 |
| 29 | -6.799216838 | 110.5462659 | 3.1093 | 33.04406 |
| 30 | -6.801816332 | 110.5439353 | 3.1434 | 29.14401 |
| 31 | -6.804236551 | 110.5424114 | 2.1404 | 4.82188 |
| 32 | -6.806343038 | 110.5402377 | 2.6173 | 5.03461 |
| 33 | -6.808494343 | 110.5390276 | 1.8534 | 0.78001 |

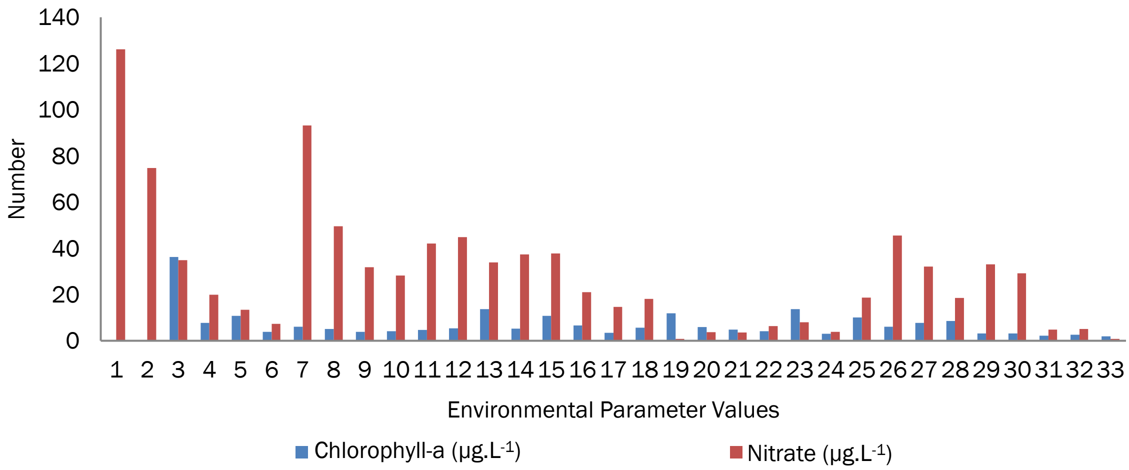


**Figure 4.** Spatial Trophic Classification of The Research Area based on Water Fertility Indicators

where restrictions on land use and enhanced protection measures may be considered. In contrast, areas with moderate vulnerability and higher trophic status reflect conditions where ecological functions remain relatively stable, suggesting that these zones may support more adaptive and ecosystem-based management approaches.

These findings are intended to support early-stage spatial planning considerations rather than to define operational management strategies and also to illustrates how combinations of physical vulnerability and trophic conditions can be interpreted to inform general management directions, such as protection, adaptation, or sustainable

**Table 4.** TSI Analysis: Trophic Classification

| Station | Chlorophyll-a (μg.L$^{-1}$) | Classification Chlorophyll-a | Nitrate (μg.L$^{-1}$) | Classification Nitrate | Conclusion of Trophic Classification (Combined) |
|---|---|---|---|---|---|
| 1 | - | Oligotrophic | 126.07798 | Oligotrophic | - |
| 2 | - | Oligotrophic | 74.73914 | Oligotrophic | - |
| 3 | 36.1936 | Eutrophic | 34.88772 | Oligotrophic | Eutrophic (Chlorophyll-a Dominant) |
| 4 | 7.6882 | Eutrophic | 19.8548 | Oligotrophic | Eutrophic (Chlorophyll-a Dominant) |
| 5 | 10.7785 | Eutrophic | 13.40199 | Oligotrophic | Eutrophic (Chlorophyll-a Dominant) |
| 6 | 3.8732 | Mesotrophic | 7.37464 | Oligotrophic | Mesotrophic (Dominant Chlorophyll-a) |
| 7 | 6.067 | Mesotrophic | 93.24665 | Oligotrophic | Mesotrophic (Dominant Chlorophyll-a) |
| 8 | 5.0791 | Mesotrophic | 49.56609 | Oligotrophic | Mesotrophic (Dominant Chlorophyll-a) |
| 9 | 3.8573 | Mesotrophic | 31.76768 | Oligotrophic | Mesotrophic (Dominant Chlorophyll-a) |
| 10 | 4.1131 | Mesotrophic | 28.29309 | Oligotrophic | Mesotrophic (Dominant Chlorophyll-a) |
| 11 | 4.6379 | Mesotrophic | 42.12054 | Oligotrophic | Mesotrophic (Dominant Chlorophyll-a) |
| 12 | 5.3333 | Mesotrophic | 44.88603 | Oligotrophic | Mesotrophic (Dominant Chlorophyll-a) |
| 13 | 13.7456 | Eutrophic | 33.89498 | Oligotrophic | Eutrophic (Chlorophyll-a Dominant) |
| 14 | 5.2841 | Mesotrophic | 37.36957 | Oligotrophic | Mesotrophic (Dominant Chlorophyll-a) |
| 15 | 10.7244 | Eutrophic | 37.79503 | Oligotrophic | Eutrophic (Chlorophyll-a Dominant) |
| 16 | 6.6889 | Mesotrophic | 20.98936 | Oligotrophic | Mesotrophic (Dominant Chlorophyll-a) |
| 17 | 3.482 | Mesotrophic | 14.67837 | Oligotrophic | Mesotrophic (Dominant Chlorophyll-a) |
| 18 | 5.594 | Mesotrophic | 18.08205 | Oligotrophic | Mesotrophic (Dominant Chlorophyll-a) |
| 19 | 11.952 | Eutrophic | 0.85092 | Oligotrophic | Eutrophic (Chlorophyll-a Dominant) |
| 20 | 5.9078 | Mesotrophic | 3.68732 | Oligotrophic | Mesotrophic (Dominant Chlorophyll-a) |
| 21 | 4.8741 | Mesotrophic | 3.61641 | Oligotrophic | Mesotrophic (Dominant Chlorophyll-a) |
| 22 | 4.0938 | Mesotrophic | 6.31099 | Oligotrophic | Mesotrophic (Dominant Chlorophyll-a) |
| 23 | 13.6926 | Eutrophic | 7.94192 | Oligotrophic | Eutrophic (Chlorophyll-a Dominant) |
| 24 | 2.9572 | Oligotrophic | 3.90005 | Oligotrophic | Oligotrophic |
| 25 | 10.1307 | Eutrophic | 18.72024 | Oligotrophic | Eutrophic (Chlorophyll-a Dominant) |
| 26 | 6.0972 | Mesotrophic | 45.52422 | Oligotrophic | Mesotrophic (Dominant Chlorophyll-a) |
| 27 | 7.6922 | Eutrophic | 32.12223 | Oligotrophic | Eutrophic (Chlorophyll-a Dominant) |
| 28 | 8.5225 | Eutrophic | 18.50751 | Oligotrophic | Eutrophic (Chlorophyll-a Dominant) |
| 29 | 3.1093 | Mesotrophic | 33.04406 | Oligotrophic | Mesotrophic (Dominant Chlorophyll-a) |
| 30 | 3.1434 | Mesotrophic | 29.14401 | Oligotrophic | Mesotrophic (Dominant Chlorophyll-a) |
| 31 | 2.1404 | Oligotrophic | 4.82188 | Oligotrophic | Oligotrophic |
| 32 | 2.6173 | Oligotrophic | 5.03461 | Oligotrophic | Oligotrophic |
| 33 | 1.8534 | Oligotrophic | 0.78001 | Oligotrophic | Oligotrophic |

utilization. However, these interpretations are indicative and should be treated with caution, as the present analysis is based on a limited set of parameters and does not explicitly incorporate dynamic processes such as land subsidence, hydrodynamic forcing, or long-term ecological variability (Farinotti *et al.,* 2015; Neal *et al.,* 2018; Nindia *et al.,* 2026).

Therefore, while the CVI–TSI integration provides useful spatial insight into relative vulnerability and ecological condition, further investigation incorporating additional physical and environmental processes is required before translating these findings into specific management interventions or policy decisions.

### *Study Limitations and Future Research*

Several limitations should be considered when interpreting the results of this study. First, the CVI assessment is based on a weighted overlay approach in which parameter importance is determined from published literature rather than site-specific calibration, introducing uncertainty in the relative contribution of individual variables. Second, the spatial resolution of the DEM and satellite imagery may influence the representation of fine-scale coastal features. Third, trophic status was evaluated using chlorophyll-a and nitrate concentrations obtained during two sampling periods, which provide representative conditions but may not fully capture seasonal and interannual variability. Finally, dynamic coastal processes such as land subsidence, wave climate, sediment transport, and hydrodynamic forcing were not explicitly incorporated into the assessment. Future studies should integrate these processes with long-term monitoring and quantitative uncertainty analyses to improve the robustness of coastal vulnerability assessment.

This study provides a baseline spatial assessment of coastal vulnerability and trophic conditions in Betahwalang Waters. However, the results are subject to uncertainty associated with the weighting of CVI parameters, spatial resolution of DEM and satellite imagery, and the omission of dynamic forcing factors such as land subsidence,

**Table 5.** CVI Analysis: Vulnerability Class Distribution

| CVI category | CVI Value | Area (Ha) | % of area |
|---|---|---|---|
| Not Vulnerable | < 0.8 | 32.279921 | 0.530207511 |
| Low Vulnerability | 0.8 - 1.55 | 1051.173442 | 17.26584318 |
| Medium Vulnerability | 1.55 > KP ≤ 2.37 | 803.713204 | 13.20123358 |
| High Vulnerability | 2.37 > KP ≤ 3.95 | 2615.268373 | 42.95657767 |
| Very High Vulnerability | > 3.95 | 1585.732495 | 26.04613805 |

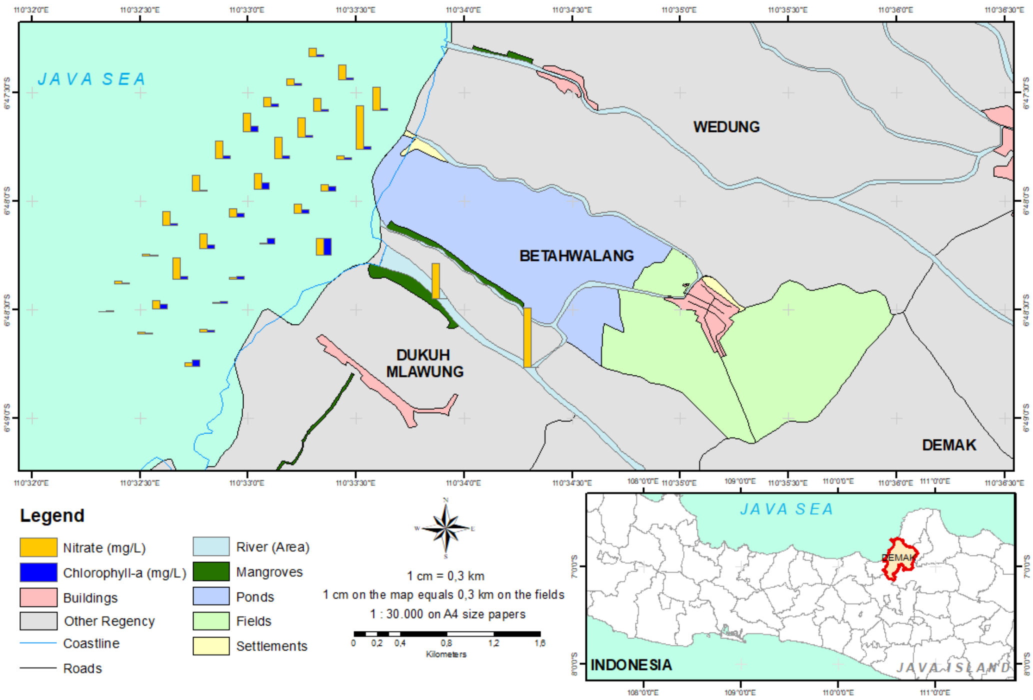


**Figure 5.** Trophic Classification of Betahwalang Water

wave climate, sediment transport, and seasonal hydrodynamic variability. Future studies should incorporate quantitative validation techniques, including sensitivity and uncertainty analyses, together with long-term monitoring datasets to further improve the robustness of the proposed assessment framework.

### *Critical interpretation & comparison*

The predominance of high coastal vulnerability observed in Betahwalang is consistent with previous studies conducted along the northern coast of Java, where low elevation, gentle coastal slopes, and extensive land-use conversion have been identified as the principal drivers of tidal flooding and shoreline degradation (Marfai and King, 2008; Sugianto *et al.,* 2022; Zainuri *et al.,* 2024). Similarly, the trophic conditions identified in this study agree with reports from other aquaculture-dominated tropical coastal waters, where nutrient enrichment is strongly associated with riverine discharge and anthropogenic activities (Nguyen *et al.,* 2019; Harding *et al.,* 1999). However, unlike previous studies that evaluated physical vulnerability or water quality separately, the present study integrates both components to provide a more comprehensive perspective for supporting ecosystem-based coastal management.

### *Synthesis*

Overall, the integration of CVI and trophic classification offers a powerful framework for understanding the dual challenges of physical vulnerability and ecological stress in tropical coastal zones (Table 5 and Figure 5). The Betahwalang case highlights how human activities, geomorphological conditions, and hydro-oceanographic processes interact to shape vulnerability and productivity patterns. The findings provide valuable insight for designing adaptive, ecosystem-based coastal management strategies in Demak and similar low-lying coastal regions (Cheong *et al.,* 2013; Temmerman *et al.,* 2013; Barbier, 2015; Narayan *et al.,* 2016).

## Conclusion

This study integrated the Coastal Vulnerability Index (CVI) and trophic classification analysis to assess physical vulnerability and aquatic productivity in the Betahwalang coastal zone, Demak. The CVI results indicated that most areas were categorized as high to very high vulnerability, driven by low elevation, gentle slopes, shoreline and river proximity, and the dominance of fishponds over mangrove vegetation, increasing exposure to tidal flooding, erosion, and saltwater intrusion (de Sousa Júnior *et al.,* 2025; Marfai and King, 2008; Zainuri *et al*., 2022; Zainuri *et al.,* 2024). Trophic assessment based on chlorophyll-a and nitrate concentrations showed mesotrophic to eutrophic conditions, reflecting nutrient enrichment from aquaculture activities and riverine inputs, which may enhance productivity but also increase the risk of eutrophication and water quality degradation if unmanaged (Carlson, 1977; Widiaratih *et al.,* 2022; Noviantoro *et al.,* 2024; Zainuri *et al*., 2026). The integration of CVI and trophic status provides a comprehensive framework for identifying areas requiring sustainable interventions, including mangrove restoration, aquaculture management, spatial zoning, and nature-based solutions to strengthen coastal resilience under climate change and sea-level rise (Cheong *et al.,* 2013). Overall, the integration of CVI and trophic status provides a more comprehensive framework for identifying priority areas for disaster mitigation and sustainable coastal management by simultaneously considering physical vulnerability and ecological conditions. Overall, the integration of CVI and trophic status provides a more comprehensive framework for identifying priority areas for disaster mitigation and sustainable coastal management by simultaneously considering physical vulnerability and ecological conditions.

## Acknowledgement

This research was funded by a research grant from the Ministry of Higher Education, Science and Technology, under contract number: 359-100/UN7.D2.1/PP/VI/2025. Additionally, this research was also funded by Universitas Diponegoro under Contract No. 306-299/UN7.D2/PP/V/2026. We would like to express our deep gratitude to the research grant from the Ministry of Higher Education, Science and Technology, as well as to all the researchers fundamental support to this study. Moreover, we would like to extend our thanks to the Diponegoro University for the provided research space and their continued institutional support. This study is a testament to the scientific community's collaboration and commitment to advancing our understanding of coastal rehabilitation and disaster mitigation studies. Finally, we would like to thank the anonymous reviewers for their revisions and suggestions, which have made this work even more complete.

## References

Ahmad, M.T. & Haie, N. 2018. Assessing the impacts of population growth and climate change on performance of water use systems and water allocation in Kano river basin, Nigeria. *Water*, 10(12): 1766. https://doi.org/10.3390/w10121766

Alongi, D.M. 2008. Mangrove forests: resilience, protection from tsunamis, and responses to global climate change. *Estuar. Coast. Shelf Sci.*, 76(1): 1–13. https://doi.org/10.1016/j.ecss.2007.08.024

American Public Health Association (APHA). 2012. *Standard methods for the examination of water and wastewater*. American Public Health Association.

Anderson, D.M., Glibert, P.M. & Burkholder, J.M. 2002. Harmful algal blooms and eutrophication: nutrient sources, composition, and consequences. *Estuaries*, 25(4): 704–726. https://doi.org/10.1007/BF02804901

Anthony, E.J., Brunier, G., Besset, M., Goichot, M., Dussouillez, P. & Nguyen, V.L. 2015. Linking rapid erosion of the Mekong River delta to human activities. *Sci. Rep.*, 5(1): 14745.

Appeaning Addo, K. 2011. Changing morphology of Ghana's Accra coast. *J. Coast. Conserv.*, 15(4): 433–443. https://doi.org/10.1007/s11852-010-0134-z

Ariffin, E.H., Mathew, M.J., Roslee, A., Ismailluddin, A., Yun, L.S., Putra, A.B. & Siddiqui, N.A. 2023. A multi-hazards coastal vulnerability index of the east coast of Peninsular Malaysia. *Int. J. Disaster Risk Reduct.*, 84: 103484. https://doi.org/10.1016/j.ijdrr.2022.103484

Azizah, R., Malau, R., Susanto, A.B., Santosa, G.W., Hartati, R., Irwani, I. & Suryono, S. 2018. Kandungan timbal pada air, sedimen, dan rumput laut *Sargassum* sp. di perairan Jepara, Indonesia. *J. Kelaut. Trop.*, 21(2): 155–156. https://doi.org/10.14710/jkt.v21i2.3010

Bailey, S.W. 2005. An improved bio-optical data set for ocean color algorithm development and satellite data product variation. *Remote Sens. Environ.*, 98(1): 122–140.

Barbier, E.B. 2016. The protective service of mangrove ecosystems: a review of valuation methods. *Mar. Pollut. Bull.*, 109(1): 676–681. https://doi.org/10.1016/j.marpolbul.2016.01.033

Basuki, T.M., Indrawati, D.R., Nugroho, H.Y.S.H., Pramono, I.B., Setiawan, O., Nugroho, N.P., Nada, F.M.H., Nandini, R., Savitri, E., Adi, R.N. & Purwanto, P. 2024. Water pollution of some major rivers in Indonesia: the status, institution, regulation, and recommendation for its mitigation. *Pol. J. Environ. Stud.*, 33(4): 3515–3530.

Blum, M.D. & Roberts, H.H. 2009. Drowning of the Mississippi Delta due to subsidence and sea-level rise. *Nat. Geosci.*, 2: 488–491. https://doi.org/10.1038/ngeo553

Bosboom, J. & Stive, M.J. 2015. *Coastal dynamics I*. ISBN 978-6562-3720.

Bouwman, A.F., Beusen, A.H.W. & Billen, G. 2009. Human alteration of the global nitrogen and phosphorus soil balances for the period 1970–2050. *Glob. Biogeochem. Cycles*, 23(4): GB0A04. https://doi.org/10.1029/2009GB003576

Capobianco, M., Larson, M. & Hanson, H. 2002. Modelling of coastal evolution on yearly to decadal time scales. *J. Coast. Res.*, 18(4): 676–689. https://www.jstor.org/stable/4299221

Carlson, R.E. 1977. A trophic state index for lakes. *Limnol. Oceanogr.*, 22(2): 361–369. https://doi.org/10.4319/lo.1977.22.2.0361

Castro, N., Ramalhosa, P., Jiménez, J., Costa, J.L., Gestoso, I. & Canning-Clode, J. 2020. Exploring marine invasions connectivity in a NE Atlantic Island through the lens of historical maritime traffic patterns. *Reg. Stud. Mar. Sci.*, 37: 101333. https://doi.org/10.1016/j.rsma.2020.101333

Cheong, S.-M., Silliman, B., Wong, P.P., Van Wesenbeeck, B., Kim, C.K. & Guannel, G. 2013. Coastal adaptation with ecological engineering. *Nat. Clim. Chang.*, 3(9): 787–791.

Cloern, J.E. 2001. Our evolving conceptual model of the coastal eutrophication problem. *Mar. Ecol. Prog. Ser.*, 210: 223–253. https://doi.org/10.3354/meps210223

Couvillion, B.R., Beck, H., Schoolmaster, D. & Fischer, M. 2017. Land area change in coastal Louisiana (1932 to 2016). *U.S. Geol. Surv. Sci. Investig. Map*, 3381: 1–16. https://doi.org/ 10.3133/sim3381

de Sousa Júnior, P.G., dos Santos, K.M., Silva, D.E.P., Nascimento Dari, D., Andrade Lima, V.D.J., da Silva Aires, F.I., de Castro Bizerra, V., Miranda Nunes, F. & Sousa dos Santos, J.C. 2025. Microbial enzymatic pathways for petroleum biodegradation in aquatic environments: molecular mechanisms and environmental perspectives. *ACS EST Water*, 5(11): 6217–6245.

Darmawan, M., Sutrisno, D., Dewi, C. & Setiyawan, I.E. 2021. The integration of regional spatial planning (RTRW) and coastal spatial planning (RZWP3K) for the sustainable coastal area development. *IOP Conf. Ser. Earth Environ. Sci.*, 750(1): 012052.

Dong, B., Ye, Y., You, S., Zheng, Q., Huang, L., Zhu, C., Tong, C., Li, S., Li, Y. & Wang, K. 2021. Identifying and classifying shrinking cities using long-term continuous night-time light time series. *Remote Sens.*, 13(16): 3142. https://doi.org/10.3390/rs13163142

Ehler, C. & Douvere, F. 2009. *Marine spatial planning: a step-by-step approach from a vision to reality*. UNESCO.

Ehrhardt, M. 1999. *Methods of seawater analysis*. Wiley-VCH.

Farinotti, D., Longuevergne, L., Moholdt, G., Duethmann, D., Mölg, T., Bolch, T., Vorogushyn, S. & Güntner, A.,2015. Substantial glacier mass loss in the Tien Shan over the past 50 years. *Nat. Geosci.*, 8: 716–722. https://doi.org/10.1038/ngeo2513

Furlan, E., Dalla Pozza, P., Michetti, M., Torresan, S., Critto, A. & Marcomini, A. 2021. Development of a multi-dimensional coastal vulnerability index: assessing vulnerability to inundation scenarios in the Italian coast. *Sci. Total Environ.*, 772: 144650. https://doi.org/10.1016/j.scitotenv.2020.144650

Gornitz, V. 1991. Global coastal hazards from future sea-level rise. *Palaeogeogr. Palaeoclimatol. Palaeoecol.*, 89(4): 379–398. https://doi.org/10.1016/0031-0182(91)90173-O

Hamuna, B., Sari, A.N. & Alianto, A. 2018. Kajian kerentanan wilayah pesisir ditinjau dari geomorfologi dan elevasi pesisir Kota dan Kabupaten Jayapura, Provinsi Papua. *J. Wil. Lingkung.*, 6(1): 1–14. https://doi.org/10.14710/jwl.6.1.1-14

Hammar-Klose, E.S., Pendleton, E.A., Thieler, E.R., Williams, S.J. & Norton, G.A. 2003. *Coastal vulnerability assessment of Cape Cod National Seashore (CACO) to sea-level rise*. US Geological Survey, Open File Report 02-233.

Handiani, D.N., Heriati, A. & Gunawan, W.A. 2022. Comparison of coastal vulnerability assessment for Subang regency in north coast West Java-Indonesia. *Geomat. Nat. Hazards Risk*, 13(1): 1178–1206. https://doi.org/10.1080/19475705.2022.2066573

Howarth, R.W., Marino, R. & Lane, J. 1988. Nitrogen fixation in freshwater, estuarine, and marine ecosystems. 1. Rates and importance. *Limnol. Oceanogr.*, 33(4part2): 668–687. https://doi.org/10.4319/lo.1988.33.4_part_2.0669

Hu, C., Lee, Z. & Franz, B. 2012. Chlorophyll a algorithms for oligotrophic oceans: a novel approach based on three-band reflectance difference. *J. Geophys. Res. Oceans*, 117(C1): C01011. https://doi.org/10.1029/2011JC007395

Irsadi, A., Anggoro, S. & Soeprobowati, T.R. 2019. Environmental factors supporting mangrove ecosystem in Semarang-Demak Coastal Area. *E3S Web Conf.*, 125: 01021. https://doi.org/10.1051/e3sconf/201912501021

Isdianto, A., Kurniasari, D., Subagiyo, A., Haykal, M.F. & Supriyadi, S. 2021. Pemetaan kerentanan tsunami untuk mendukung ketahanan wilayah pesisir. *J. Permukiman*, 16(2): 90. https://doi.org/10.31815/jp.2021.16.90-100

Karasius, I., Putri, D.E., Mariati, H. & Febrianto, H. 2024. Analisis tingkat dan faktor penyebab kerawanan banjir di Kecamatan Siberut Selatan. *J. Georafflesia Artik. Ilm. Pendidik. Geogr.*, 9(1): 1–9.

Marfai, M.A. & King, L. 2008. Tidal inundation mapping under enhanced land subsidence in Semarang, Central Java Indonesia. *Nat. Hazards*, 44(1): 93–109. https://doi.org/10.1007/s11069-007-9144-z

Ma'rufatin, A., Yananto, A. & Pandoe, W.W. 2024. Karakteristik angin wilayah pesisir utara Pulau Jawa berdasarkan variabilitas monsun. *J. Teknol. Lingkung.*, 25(1): 20–30. https://doi.org/10.55981/jtl.2024.2039

Maulina, I. & Sulastri, S. 2020. Eutrofikasi: hijau tidak selalu lestari. *J. Ilmu Lingkung.*, 18(2): 331–340.

McLachlan, A. & Dorvlo, A. 2005. Global patterns in sandy beach macrobenthic communities. *J. Coast. Res.*, 21(4): 674–687. https://doi.org/10.2112/03-0114.1

Mishra, M., Kar, P.K., Chand, P., Mohanty, P.K., Acharyya, T., Santos, C.A.G., [penulis lainnya dilengkapi] & Behera, B. 2023. Deciphering the impact of anthropogenic coastal infrastructure on shoreline dynamicity along Gopalpur coast of Odisha (India): an integrated assessment with geospatial and field-based approaches. *Sci. Total Environ.*, 858: 159625.

Monbet, Y. 1992. Control of phytoplankton biomass in estuaries: a comparative analysis of microtidal and macrotidal estuaries. *Estuaries*, 15(4): 563–571.

Narayan, S., Beck, M.W., Reguero, B.G., Losada, I.J., van Wesenbeeck, B., Pontee, N., Sanchirico, J.N., Ingram, J.C., Lange, G.-M. & Burks-Copes, K.A. 2016. The effectiveness, costs and coastal protection benefits of natural and nature-based defenses. *PLoS One*, 11(5): e0154735. https://doi.org/10.1371/journal.pone.0154735

Neal, W.J., Pilkey, O.H., Cooper, J.A.G. & Longo, N.J. 2018. Why coastal regulations fail. *Ocean Coast. Manag.*, 156: 21–34. https://doi.org/10.1016/j.ocecoaman.2017.05.003

Nindia, M.N., Hanum, A.F.F. & Rohmah, L.T. 2026. Hubungan spasial parameter geologi bawah permukaan dan kualitas air tanah untuk memahami intrusi air laut di Cekungan Semarang: spatial integration of subsurface geological parameters and groundwater quality to understand seawater intrusion in the Semarang Basin. *J. Tek. Sumber Daya Air*: 29–40. https://doi.org/10.56860/jtsda.v6i1.130

Noviantoro, K.M., Firnanda, A., Sari, D.N. & Fajri, Y.T. 2024. Potensi dan peluang pengembangan usaha perikanan berkelanjutan dalam meningkatkan perekonomian masyarakat Pulau Bawean Gresik. *Din. Sos. J. Pendidik. Ilmu Pengetahuan Sos.*, 3(3): 223–237.

Nurul, R., Sagala, S., Arya, A., Krismiyaningsih, E. & Adinta, U.N. 2025. Between adaptation or retreat in the face of slow-onset disasters: lessons learned of Indonesia's national and local adaptation strategies to manage displacement risks. *IOP Conf. Ser. Earth Environ. Sci.*, 1479(1): 012050.

Pardo-Pascual, J.E., Almonacid-Caballer, J., Ruiz, L.A. & Palomar-Vázquez, J. 2012. Automatic extraction of shorelines from Landsat TM and ETM+ multi-temporal images with subpixel precision. *Remote Sens. Environ.*, 123: 1–11. https://doi.org/10.1016/j.rse.2012.02.024

Parsons, T.R., Maita, Y. & Lalli, C. 1984. *A manual of chemical and biological methods for seawater analysis*. Pergamon Press. https://doi.org/10.1016/C2009-0-07774-5

Ramadhani, A.R. 2025. Kerentanan kawasan pesisir Kota Palu berdasarkan ancaman bencana tsunami (studi kasus: Kecamatan Mantikulore).

Undergraduate thesis, Universitas Hasanuddin, Makassar.

Ridarto, N.B.H., Setiawati, M., Fauzi, I.A., Jusadi, D., Ekasari, J., Adestia, T.S. & Suprayudi, M.A. 2026. Evaluation of manganese supplementation in feed on growth performance and antioxidant response of tilapia *Oreochromis* sp. *Egypt. J. Aquat. Biol. Fish.*, 30(3): 3381–3398. https://doi.org/10.19027/jai.2.27-30

Rimba, A.B., Osawa, T., Parwata, I.N.S., As-syakur, A.R., Kasim, F. & Astarini, I.A. 2018. Physical assessment of coastal vulnerability under enhanced land subsidence in Semarang, Indonesia, using multi-sensor satellite data. *Adv. Space Res.*, 61(8): 2159–2179. https://doi.org/10.1016/j.asr.2018.01.026

Ringor, C.L. & Siringan, F.P. 2016. Net sediment transport in Pampanga Bay, northwestern Manila Bay derived from grain size trends, bathymetric change and Landsat data. *Philipp. Agric. Sci.*, 99(1): 68–79. https://doi.org/10.62550/CR6879

Sarwar, M.G.M. & Woodroffe, C.D. 2013. Rates of shoreline change along the coast of Bangladesh. *J. Coast. Conserv.*, 17(3): 515–526. https://doi.org/10.1007/s11852-013-0251-6

Shi, Z., Ren, L.F. & Hamilton, L.J. 1999. Acoustic profiling of fine suspension concentration in the Changjiang Estuary. *Estuaries*, 22(3): 648–656. https://doi.org/10.2307/1353052

Siegel, H. & Gerth, M. 2008. Optical remote sensing applications in the Baltic Sea. In: *Remote sensing of the European seas*. Springer, Dordrecht. pp. 91–102. https://doi.org/10.1007/978-1-4020-6772-3_7

Simbolon, A.R. 2016. Pencemaran bahan organik dan eutrofikasi di perairan Cituis, Pesisir Tangerang. *Pro-Life*, 3(2): 109–118.

Sugianto, D.N., Widiaratih, R., Widada, S., Suripin, S., Handayani, E.P. & Cahyaningtyas, P. 2022. Analysis of structural and non-structural disaster mitigation due to erosion in the Timbulsloko Village, Demak–Central Java. *J. Ecol. Eng.*, 23(2): 246–254. https://doi.org/10.12911/22998993/144559

Temmerman, S., Meire, P., Bouma, T.J., Herman, P.M., Ysebaert, T. & De Vriend, H.J. 2013. Ecosystem-based coastal defence in the face of global change. *Nature*, 504(7478): 79–83. https://doi.org/10.1038/nature12859

Thanjaya, R.D.C. & Saputra, A. 2021. *Analisis risiko sosial bencana banjir rob di pesisir Kabupaten Demak*. Doctoral dissertation, Universitas Muhammadiyah Surakarta.

Valdez-Rojas, C., Beas-Luna, R., Lorda, J., Zepeda-Domínguez, J.A., Montáño-Moctezuma, G., Medellín-Ortíz, A., Torre, J. & Micheli, F. 2022. Using a social-ecological systems perspective to identify context specific actions to build resilience in small scale fisheries in Mexico. *Front. Mar. Sci.*, 9: 904859. https://doi.org/10.3389/fmars.2022.904859

Widiaratih, R., Suryoputra, A.A.D. & Handoyo, G. 2022. Korelasi klorofil-a dengan nutrien dan kualitas perairan di Pulau Seruni Karimunjawa Indonesia. *J. Kelaut. Trop.*, 25(2): 249–256. https://doi.org/10.14710/jkt.v25i2.14170

Wieder, W., Bonan, G. & Allison, S. 2013. Global soil carbon projections are improved by modelling microbial processes. *Nat. Clim. Chang.*, 3: 909–912. https://doi.org/10.1038/nclimate1951

Wirasatriya, A., Sugianto, D.N., Helmi, M., Setiawan, R.Y. & Koch, M. 2019. Distinct characteristics of SST variabilities in the Sulawesi Sea and the northern part of the Maluku Sea during the southeast monsoon. *IEEE J. Sel. Top. Appl. Earth Obs. Remote Sens.*, 12(6): 1763–1770. https://doi.org/10.1109/JSTARS.2019.2913739

Woodruff, J.D., Irish, J.L. & Camargo, S.J. 2013. Coastal flooding by tropical cyclones and sea-level rise. *Nature*, 504(7478): 44–52.

Yentsch, C.S. & Menzel, D.W. 1963. A method for the determination of phytoplankton chlorophyll and phaeophytin by fluorescence. *Deep Sea Res. Oceanogr. Abstr.*, 10(3): 221–231. https://doi.org/10.1016/0011-7471(63)9035 8-9

Zainuri, A., Lihawa, F., Baderan, D.W.K., Mahmud, M. & Yusuf, D. 2024. Analisis bibliometrik penelitian intrusi air laut di estuari. *J. Biogenerasi*, 9(1): 916–922.

Zainuri, M., Helmi, M., Novita, M.G.A., Kusumaningrum, H.P. & Koch, M. 2022. Improved performance of geospatial model to access the tidal flood impact on land use by evaluating sea level rise and land subsidence parameters. *J. Ecol. Eng.*, 23(2): 1–11. https://doi.org/10.12911/22998993/144785

Zainuri, M., Candrasekar, A.R., Kunarso, K., Rochaddi, B., [nama tidak jelas], Sasmita, S.A., Febriyanti, A.P. & Susilowati, A. 2026. Assessment and characterization of water quality and pollution in the coastal environment of Pekalongan, Central Java, Indonesia. *Geographia Technica*, 21(1): 288–305. https://doi.org/10.21163/GT2026.211.19